Nano Energy (2015) 12, 606–611

Available online at www.sciencedirect.com

ScienceDirect

journal homepage: www.elsevier.com/locate/nanoenergy

RAPID COMMUNICATION

Fully enclosed bearing-structured self-powered rotation sensor based on electrification at rolling interfaces for multi-tasking motion measurement

Xian Song Meng[a], Hua Yang Li[a], Guang Zhu[a,*], Zhong Lin Wang[a,b,*]

[a]*Beijing Institute of Nanoenergy and Nanosystems, Chinese Academy of Sciences, Beijing 100083, China*
[b]*School of Material Science and Engineering, Georgia Institute of Technology, Atlanta, GA 30332, United States*

Received 20 November 2014; received in revised form 26 December 2014; accepted 8 January 2015
Available online 24 January 2015

KEYWORDS
Triboelectric effect;
Self-powered sensing;
Motion sensor;
Energy conversion

Abstract
A fully enclosed bearing-structured self-powered rotation sensor (SPRS) is developed for multi-tasking motion measurement. Due to contact electrification between fine-sized rolling beads and a pair of planar electrodes, the SPRS produce cycled electric signals when attached to a revolving axis. They are then analyzed to reveal the rotation rate of the axis and other corresponding derivable parameters, including speed, acceleration, and traveling distance. The device displays high precision, broad range, quick response, and excellent durability. It has novel dual roles as a rotation sensor and a structural ball bearing, making it easily applicable to a variety of circumstances. Integrated with a signal-processing interface, the compact-sized and light weighted SPRS was practically demonstrated in providing real-time motion monitoring for a vehicle wheel. It is promised to be used in a wide range of areas, including transportation, automation, consumer products, and industrial monitoring.

Introduction

Triboelectric effect is receiving increasingly extensive attentions as fueled by its recently explored novel applications in energy harvesting [1–5], self-assembly [6,7], chemical process [8,9], x-ray emission [10,11], and self-powered sensing [12–14]. For a triboelectric sensor, electric signals are

*Corresponding authors at: Beijing Institute of Nanoenergy and Nanosystems, Chinese Academy of Sciences, Beijing 100083, China.
E-mail addresses: zhuguang@binn.cas.cn (G. Zhu), zlwang@binn.cas.cn (Z.L. Wang).

http://dx.doi.org/10.1016/j.nanoen.2015.01.015
2211-2855/

generated in response to intimate friction between two dissimilar materials due to the coupling effect between contact electrification and electrostatic induction, which provide quantitative insights into motion characteristics [15]. Although this type of self-powered sensors features zero-power consumption, simple structure, and low cost [16], there are important issues yet to be solved. First of all, the friction causes mechanical wear of materials [15,17], posing a challenge to longevity and stability of the sensor. Second, most of them could only reveal a particular parameter [15], which is insufficient for characterizing the motion in a well-rounded way. Besides, previously reported triboelectric sensors consist of separate components, which may lead to installation difficulties [18].

In this work, by utilizing contact electrification between fine-sized rolling beads and a pair of planar electrodes, we develop a fully enclosed, bearing-structured and self-powered rotation sensor (SPRS) for multi-tasking motion measurement. When the SPRS is attached to a revolving axis, the periodically positioned beads produce cycled electric signals. They are then analyzed to reveal the rotation rate of the axis and other corresponding derivable motion parameters, including speed, acceleration, and traveling distance. The SPRS displays high precision, broad range, and quick response. The rolling interaction minimizes the mechanical friction, which enables excellent durability and stability of the device. Due to the rationally designed structure, the SPRS has novel dual roles as a rotation sensor and a structural ball bearing. This feature brings about simplicity and convenience in implementation. Integrated with a signal-processing interface, the compact-sized and light weighted SPRS was practically demonstrated in providing real-time motion monitoring for a vehicle wheel. It is promising to be used in a wide range of areas, including transportation, automation, consumer products, and industrial monitoring.

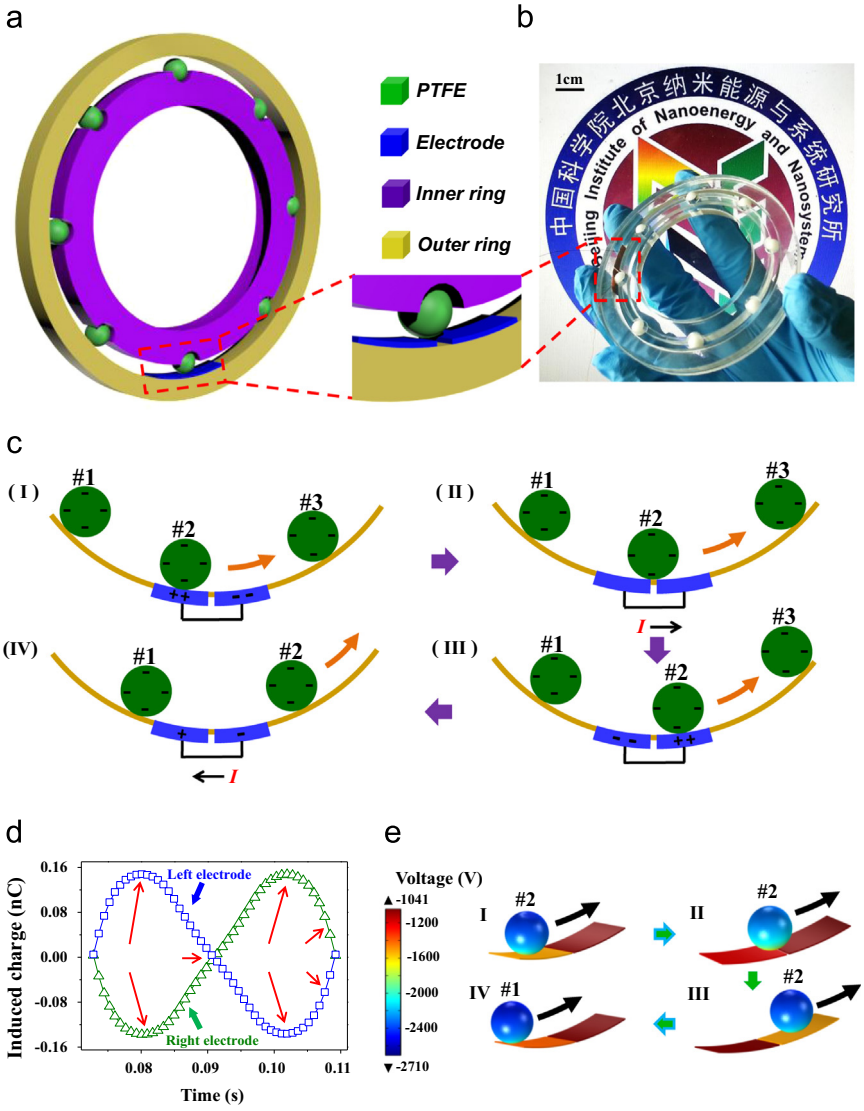

Fig. 1 Structure and operating principle of a SPRS. (a) Schematic diagram and (b) photograph of the device. The enlarged view in (a) shows the details of the electrodes. (c) Schematics that illustrate the flow of induced charges between the electrodes when negatively charged beads are rolling over. (d) Variance of charge distribution calculated by COMSOL on the two electrodes in a complete cycle. The distribution that corresponds to the four states in (c) is pointed out by red arrows. (e) Simulation results of electric potential in open-circuit condition as the beads are rolling over the electrode pair. The four states correspond to those in (c).

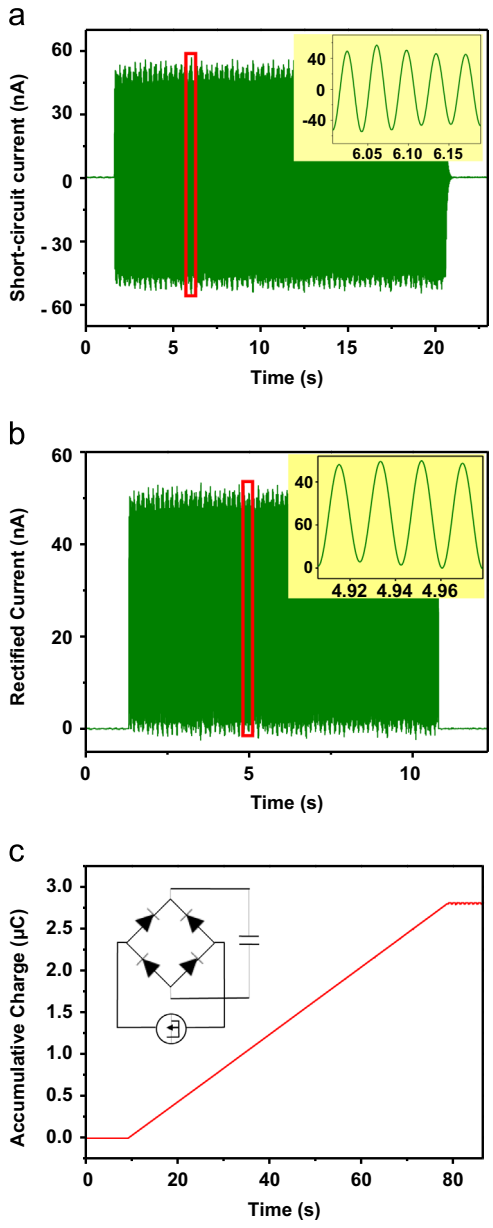

Fig. 2 Electric signals generated by the SPRS when driven by an electric motor at a rotation rate of 206 rpm. (a) Short-circuit current. Inset: enlarged view enclosed by the red frame. (b) Rectified current without an extra load. Inset: enlarged view enclosed by the red frame. (c) Absolute value of induced charge from the rectified current in (b). Inset: circuit diagram of the measurement.

Results and discussion

As shown in Fig. 1a, the SPRS has a double-ring structure. The acrylic inner ring has a radial array of semicircle-shaped indentations that accommodate fine-sized beads made of PTFE. Two metal electrodes deposited on plastic thin-film substrates are adhered on the inner wall of the outer ring (enlarged inset in Fig. 1a). The two rings can have free relative rotation as enabled by the rolling beads. An as-fabricated device is shown in Fig. 1b. The fabrication details are presented in Methods. The intimate contact between the PTFE beads and the acrylic ring causes quasi-permanent charge transfer at the contact interface between the two insulating materials [20,21]. Since PTFE has a strong tendency to gain electrons [22,23], negative triboelectric charges are generated on the beads surface, leaving the acrylic ring surface positively charged. Since the metal electrodes cover only a small fraction of the outer ring surface, charge transfer between the PTFE beads and the metal electrodes can be reasonably neglected. When a revolving axis drives the inner ring, the PTFE beads roll across the electrodes in a periodic way, producing cycled electric signals. Fig. 1c uses four typical states in a complete cycle to illustrate the self-powered sensing mechanism. At the first state (I), the negative charged bead no. 2 is at the middle position of the left electrode, creating positive and negative induced charges on the left and the right electrodes, respectively. As the bead rolls from the left electrode onto the right electrode, a flow of induced current is generated towards the right-hand electrode (state II) until the bead is in alignment with the right electrode (state III). As the bead no. 2 rolls away from the right-hand electrode and the bead no. 1 approaches the left-hand electrode, another flow of current in the opposite direction is produced (state IV). As a result, each passing bead generates a pair of alternating current (ac) peaks. Numerically calculated via COMSOL, the distribution of induced charges on the two electrodes changes in a complementary way as a bead rolls over (Fig. 1d). The charge flow process can be also explained by the variance of electric potential across the two electrodes in open-circuit condition as the negatively charged beads are passing over (Fig. 1e). Detailed simulation settings are presented in Experimental section.

To quantitatively obtain the sensing characteristics of the SPRS, a programmable electric motor was used to drive the inner ring while the outer ring kept stationary. Short-circuit current (I_{sc}) measured by an electrometer (Keithley 6514) at an arbitrary rate of 206 rpm is presented in Fig. 2a. The inset in Fig. 2a exhibits an alternating pattern, which is consistent with the theoretical analysis above. The minor fluctuation in amplitude is likely attributed to the slight difference of charge density on individual beads. The ac signal can be converted into direct current simply through a full-wave rectifying bridge (Fig. 2b). The absolute value of total induced charge that flow between the electrodes is shown in Fig. 2c, which further confirms the generated current flow between the two electrodes. Therefore, the electric signal is self-generated without reliance on an external power source.

Based on the measured oscillating electric signal, detailed information of the rotation can be extracted and derived. Here, the current signal was utilized. As illustrated in Fig. 3a, 54 complete cycles were randomly selected at a measurement sampling rate of 3000 s^{-1}. Then the rotation rate can be calculated by the following equation:

$$n = \frac{N}{T_2 - T_1} \times \frac{60}{k} \quad (1)$$

where N is an integer that equals the number of cycles, T_1 and T_2 are the starting and the ending time as marked in Fig. 3a, respectively, and k is the number of PTFE beads (k=8). The calculated value of 205.88 rpm matches well with the setting value of 206 rpm on the motor.

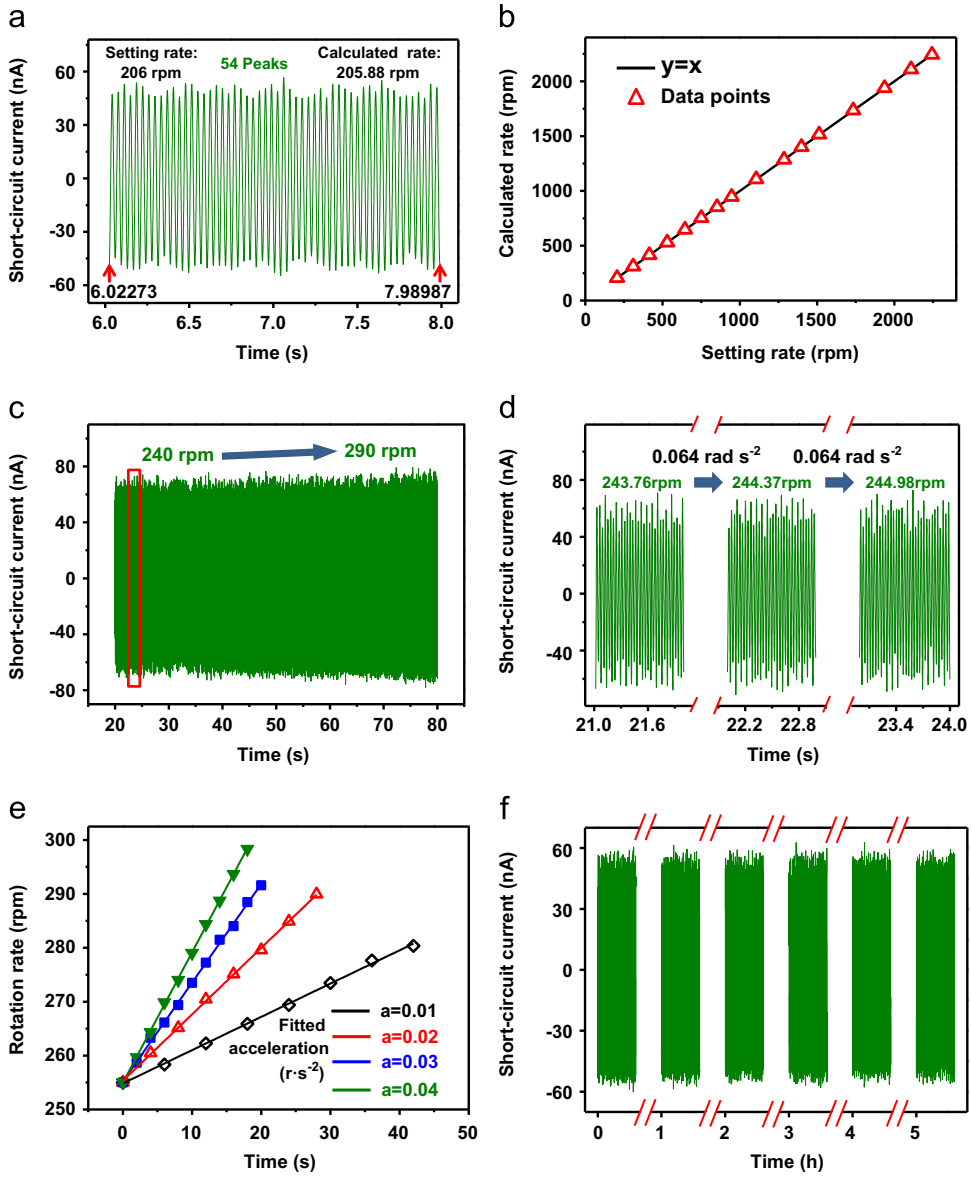

Fig. 3 Data analysis and durability of the SPRS. (a) Randomly selected 54 complete current peaks at a setting rotation rate of 206 rpm. The starting and ending times are labelled by red arrows. (b) Calculated rotation rates fit well with the setting rates from 200 rpm to 2200 rpm. (c) The current signal when the rotation rate increases from 240 rpm to 290 rpm in 60 s with a uniform acceleration. (d) Enlarged view of the current signal in a span of 3 s enclosed by the red framework in (c). It is further divided into three consecutive segments for average acceleration calculation. (e) Accelerations derived from linear fitting of multiple calculated rotation rates when the motor is set at different acceleration values. (f) Durability test of the SPRS for 5 h at a rotation rate of 230 rpm.

By the same calculation method, different rotation rates can be obtained. Fig. 3b displays a range of data points that fall exactly on the ideal linear curve of $y=x$ from 200 rpm to 2200 rpm, indicating that the calculated values fit well with the setting values. The average error is found to be only less than 0.09% (Supporting Table S1). Considering the inherent error of the electric motor ($\pm$0.1%), the SPRS has an extremely high accuracy.

Fig. 3c shows the current signal when the rotation rate of the motor increases from 240 rpm to 290 rpm in 60 s with a uniform acceleration. The slightly enhanced current amplitude is attributed to increasingly faster charge flow between the electrodes. A section of data in a span of 3 s was randomly selected from Fig. 3c and then evenly divided into three segments, as enlarged in Fig. 3d. For each segment, an average rotation rate can be calculated by Eq. (1). Then the average acceleration between two adjacent segments can be obtained (Fig. 3d), which is in exact agreement with the setting value (0.064 rad s^{-2}). As exhibited in Fig. 3e, different acceleration can be derived by linear fitting of multiple calculated rotation rates. Provided that the time span of a data segment in Fig. 3d reduces, the obtained average acceleration will increasingly approach the instantaneous acceleration. As a consequence, the ultimate time resolution in measuring the acceleration as well as the rotation rate is determined by the current period, which is then dependent on rotation rate itself.

It needs to be noted that rolling interaction between the beads and the electrodes plays a key role in enabling

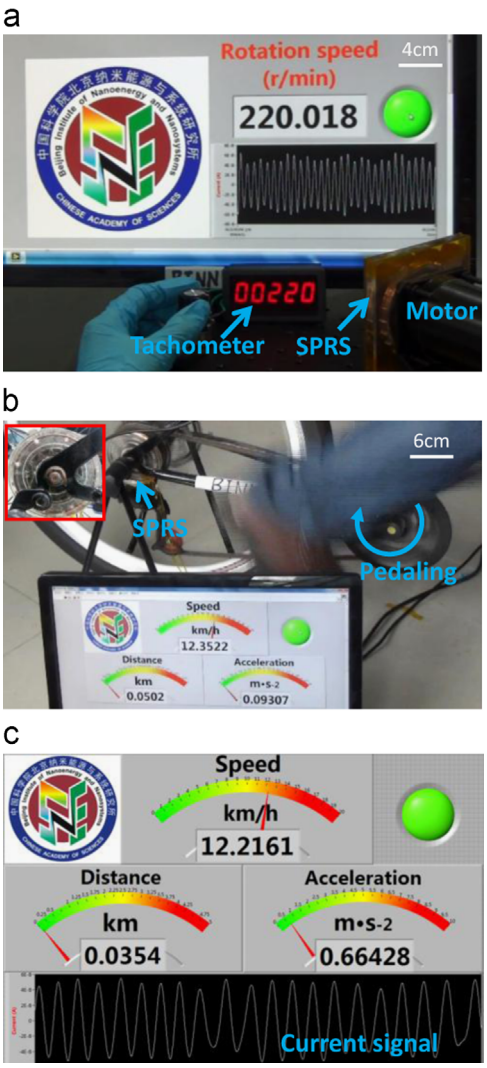

Fig. 4 Demonstrations on applications of the SPRS. (a) Real-time monitoring on the rotation rate of a motor by the SPRS and by a commercial digital tachometer simultaneously. (b) Field test of the SPRS on measuring motion parameters of a bicycle, including traveling distance, speed, and acceleration. Inset: the SPRS that is installed on the bicycle wheel. (c) The enlarged view of the display panel that show the motion parameters.

excellent robustness of the device by minimizing friction-induced wear of materials. As demonstrated in Fig. 3f, the current signal keeps constant after continuous rotation of 100 thousand rounds for 5 h, which is an important feature regarding practical applications of the device.

To demonstrate the practicability of the SPRS, the rotation rate of the motor was monitored simultaneously by the SPRS and by a commercial digital tachometer. A LabVIEW interface was built based on the same algorithm as above to exhibit the real-time measurement results of the SPRS. As shown in Fig. 4a, the rotation rate measured by the two means agrees well. The SPRS can respond much faster than the commercial tachometer once the rotation rate varies (Supporting Movie 1), indicating the ability of the SPRS in real-time monitoring. Moreover, practical field test was performed, in which the SPRS was readily installed on a bicycle wheel (inset in Fig. 4b). Since the wheel has a known diameter, multiple motion parameters of the bicycle, including traveling distance, can be immediately derived solely based on the measured oscillating electric signal. As the bicycle is being pedaled, all motion parameters are displayed on a computer monitor in real time (Fig. 4b and c, Supporting Movie 2).

Supplementary material related to this article can be found online at http://dx.doi.org/10.1016/j.nanoen.2015.01.015.

Moreover, the methodology presented in this work can be readily applied into commercial bearings made of steel, as shown in Supporting Fig. S1. The measured current signal displayed in Supporting Fig. S2 exactly resembles that shown in Fig. 2. Therefore, this work presents a viable and practical solution to a variety of circumstances with little alternation to current mechanical structures.

Experimental section

Fabrication of a SPRS

An acrylic sheet with a thickness of 6 mm was laser-cut into a ring shape, which has an outer diameter and inner diameter of 85 mm and 70 mm, respectively. This is the outer part of the SPRS. The inner part of the device has a similar shape except that eight evenly spaced indentations were created around the outer circumference to accommodate PTFE beads having a diameter of 5 mm. Two identical metal electrodes separated by a small gap of 0.5 mm were laid on the inner side of outer part. Each electrode consists of a thin-film substrate (25 um in thickness) and a deposited metal layer of 200 nm by sputtering. The electrodes cover a radian of 0.52.

Theoretical simulation via COMSOL

3D models were built according to the actual dimensions of the device. In open-circuit condition, the outer surface of the PTFE beads was assigned a surface charge density of -8×10^{-6} C m^{-2} [19]. The two planar electrodes were both assigned zero surface charge.

Conclusion

In summary, we developed a fully enclosed bearing-structured self-powered rotation sensor (SPRS) for multi-tasking motion measurement. Relying on contact electrification at the rolling interface, the SPRS features high precision, proved longevity, simple structure, and compatibility to a revolving axis. When applied onto a rolling wheel of a vehicle, it could simultaneously measure speed, acceleration, and traveling distance. This technique can be even potentially applied to commercial bearings with little alteration for an integrated and convenient measurement solution, which can have widespread applications in common fields that include industrial monitoring, automation, transportation, and consumer products.

Associated content

Supporting information

Measured rotation rates at different setting rates, structure and operating principle of a SPRS installed on the commercial

ball bearing, the SPRS performance installed on the commercial bearing. This material is available free of charge via the Internet at http://pubs.acs.org.

Competing interest

The authors declare no competing financial interest.

Acknowledgments

The research was supported by the "Thousands Talents" program for pioneer researcher and his innovation team, China, Beijing City Committee of Science and Technology project (Z131100006013004; Z131100006013005). Patents have been filed based on the research presented here.

Appendix A. Supporting information

Supplementary data associated with this article can be found in the online version at http://dx.doi.org/10.1016/j.nanoen.2015.01.015.

References

[1] Z.L. Wang, ACS Nano 7 (2013) 9533–9557.
[2] G. Zhu, J. Chen, T. Zhang, Q. Jing, Z.L. Wang, Nat. Commun. (2014). http://dx.doi.org/10.1038/ncomms4426.
[3] S. Kim, M.K. Gupta, K.Y. Lee, A. Sohn, T.Y. Kim, K.S. Shin, D. Kim, S.K. Kim, K.H. Lee, H.J. Shin, D.W. Kim, S.W. Kim, Adv. Mater. 26 (2014) 3918–3925.
[4] K.Y. Lee, J. Chun, J.H. Lee, K.N. Kim, N.R. Kang, J.Y. Kim, M.H. Kim, K.S. Shin, M.K. Gupta, J.M. Baik, Adv. Mater. (2014). http://dx.doi.org/10.1002/adma.201401184.
[5] X.S. Meng, G. Zhu, Z.L. Wang, ACS Appl. Mater. Interfaces 6 (2014) 8011–8016.
[6] B.A. Grzybowski, A. Winkleman, J.A. Wiles, Y. Brumer, G.M. Whitesides, Nat. Mater. 2 (2003) 241–245.
[7] A.M. Kalsin, B.A. Grzybowski, Nano Lett. 7 (2007) 1018–1021.
[8] C. Liu, A.J. Bard, Nat. Mater. 7 (2008) 505–509.
[9] C.-y. Liu, A.J. Bard, Chem. Phys. Lett. 480 (2009) 145–156.
[10] C.G. Camara, J.V. Escobar, J.R. Hird, S.J. Putterman, Nature 455 (2008) 1089–1092.
[11] A.L. Collins, C.G. Camara, B.B. Naranjo, S.J. Putterman, J.R. Hird, Phys. Rev. B: Condens. Matter 88 (2013) 064202.
[12] M. Han, X.-S. Zhang, X. Sun, B. Meng, W. Liu, H. Zhang, Sci. Rep. (2014). http://dx.doi.org/10.1038/srep04811.
[13] B. Meng, W. Tang, Z.-h. Too, X. Zhang, M. Han, W. Liu, H. Zhang, Energy Environ. Sci. 6 (2013) 3235–3240.
[14] X. Yang, G. Zhu, S. Wang, R. Zhang, L. Lin, W. Wu, Z.L. Wang, Energy Environ. Sci. 5 (2012) 9462–9466.
[15] Y.S. Zhou, G. Zhu, S. Niu, Y. Liu, P. Bai, Q. Jing, Z.L. Wang, Adv. Mater. 26 (2014) 1719–1724.
[16] G. Zhu, W.Q. Yang, T. Zhang, Q. Jing, J. Chen, Y.S. Zhou, P. Bai, Z.L. Wang, Nano Lett. 14 (2014) 3208–3213.
[17] L. Lin, Y. Xie, S. Wang, W. Wu, S. Niu, X. Wen, Z.L. Wang, ACS Nano 7 (2013) 8266–8274.
[18] Y. Yang, H. Zhang, J. Chen, Q. Jing, Y.S. Zhou, X. Wen, Z.L. Wang, ACS Nano 7 (2013) 7342–7351.
[19] S. Niu, Y. Liu, S. Wang, L. Lin, Y.S. Zhou, Y. Hu, Z.L. Wang, Adv. Funct. Mater. 24 (2014) 3332–3340.
[20] G.S.P. Castle, J. Electrostat. 40-41 (1997) 13–20.
[21] H. Baytekin, A. Patashinski, M. Branicki, B. Baytekin, S. Soh, B.A. Grzybowski, Science 333 (2011) 308–312.
[22] D.J. Lacks, R.M. Sankaran, J. Phys. D: Appl. Phys. 44 (2011) 453001.
[23] A. Diaz, R. Felix-Navarro, J. Electrostat. 62 (2004) 277–290.

Xian Song Meng is a graduate student at the Beijing Institute of Nanoenergy and Nanosystems, Chinese Academy of Sciences. He received his bachelor degree in Material Physics at the Hefei University of Technology in 2012. His current research mainly focuses on the energy harvesting and self-power sensor by triboelectric nanogenerator.

Hua Yang Li received his undergraduate degree from the Zhengzhou University in 2013, and his major is Materials Science and Engineering, and now he is a first-year graduate student in the Beijing Institute of Nanoenergy and Nanosystems, Chinese Academy of Sciences. His research interests are focused on triboelectric nanogenerator, preparation and modification of materials.

Dr. Guang Zhu is a professor at the Beijing Institute of Nanoenergy and Nanosystems, Chinese Academy of Sciences. He received his Ph.D. degree in Materials Science and Engineering at the Georgia Tech in 2013 and his Bachelor degree in Materials Science and Engineering at the Beijing University of Chemical Technology in 2008. His current research mainly focuses on designing, fabrication, and implementation of innovative miniaturized high-efficiency generators that harvest and convert ambient mechanical energy into electricity.

Dr. Zhong Lin Wang is a Hightower Chair and Regents's Professor at the Georgia Tech. He is also the Chief scientist and Director for the Beijing Institute of Nanoenergy and Nanosystems, Chinese Academy of Sciences. His discovery and breakthroughs in developing nanogenerators establish the principle and technological road map for harvesting mechanical energy from environment and biological systems for powering personal electronics. His research on self-powered nanosystems has inspired the worldwide effort in academia and industry for studying energy for micro-nano-systems, which is now a distinct disciplinary in energy research and future sensor networks. He coined and pioneered the field of piezotronics and piezo-phototronics by introducing piezoelectric potential gated charge transport process in fabricating new electronic and optoelectronic devices.